ORIGINAL PAPER

Characterization of the binding of angiotensin II receptor blockers to human serum albumin using docking and molecular dynamics simulation

Jinyu Li · Xiaolei Zhu · Cao Yang · Rongwei Shi

Abstract Human serum albumin (HSA), the most abundant protein found in blood plasma, transports many drugs and ligands in the circulatory system. The drug binding ability of HSA strongly influences free drug concentrations in plasma, and is directly related to the effectiveness of clinical therapy. In current work, binding of HSA to angiotensin II receptor blockers (ARBs) are investigated using docking and molecular dynamics (MD) simulations. Docking results demonstrate that the main HSA–ARB binding site is subdomain IIIA of HSA. Simulation results reveal clearly how HSA binds with valsartan and telmisartan. Interestingly, electrostatic interactions appear to be more important than hydrophobic interactions in stabilizing binding of valsartan to HSA, and vice versa for HSA–telmisartan. The molecular distance between HSA Trp214 (donor) and the drug (acceptor) can be measured by fluorescence resonance energy transfer (FRET) in experimental studies. The average distances between Trp-214 and ARBs are estimated here based on our MD simulations, which could be valuable to future FRET studies. This work will be useful in the design of new ARB drugs with desired HSA binding affinity.

Keywords Human serum albumin · Valsartan · Telmisartan · Molecular dynamics · Docking

J. Li · X. Zhu (✉) · C. Yang · R. Shi
State Key Laboratory of Materials-Oriented Chemical Engineering, College of Chemistry and Chemical Engineering, Nanjing University of Technology, Nanjing 210009, China
e-mail: xlzhu@njut.edu.cn

Introduction

Human serum albumin (HSA), the major constituent of plasma protein, plays a fundamental role in the transport of fatty acids, metabolites, and drugs. Binding to HSA is crucial for drug absorption, distribution, metabolism, and efficiency. In addition, HSA can act as a catalyst for the hydrolysis of various compounds, such as esters, amides, and phosphates [1].

The structure of HSA has been known since 1975, and the first high-resolution crystal structure of HSA was determined in 1992 [2]. HSA is comprised of 585 amino acids and has a molecular mass of 66 kDa; the secondary structure is shown in Fig. 1. HSA is composed of three homologous domains (I–III) and each domain is divided into two subdomains (A and B) that contain six and four α-helices, respectively [2, 3]. The main drug binding sites on HSA are located in subdomains IIA and IIIA [2], which are known as warfarin- (site I) and benzodiazepine- (site II) binding sites [4, 5], respectively.

Hypertension is one of the most prevalent human diseases in the developed world [6]. Angiotensin II (Ang II) plays a key role in the regulation of blood pressure and electrolyte balance. Ang II receptor blockers (ARBs) have proved to lower blood pressure effectively and have fewer side effects than other classes of antihypertensive drugs [7, 8]. Nowadays, ARBs are widely used in the treatment of hypertension and have also been found to display some other pharmacologic effects in the treatment of diabetes [9–11] and heart disease [12, 13].

So far, there are seven main ARBs on the market and their chemical structures are shown in Fig. 2. Most of these compounds have a common biphenyl fragment bearing an acidic moiety (tetrazole ring or carboxyl), but their side chains are different. The differences in molecular structures
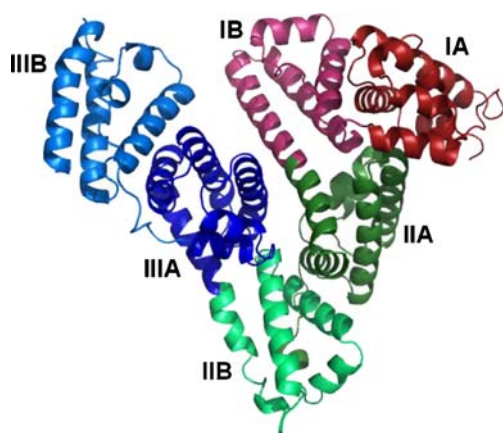
Fig. 1 Secondary structure of human serum albumin (HSA; PDB code: 1 H9Z). Domains: *Red* I, *green* II, *blue* III; A and B subdomains are depicted in *dark* and *light* shades, respectively

of ARBs result in pharmacologic and pharmacokinetic differences. All of these drugs exhibit high plasma protein binding, ranging from 95% (for valsartan) to 99.5% (for telmisartan) [14-16]. High plasma protein binding can prolong the duration of drug action. However, it also can reduce the concentration of free drug available for
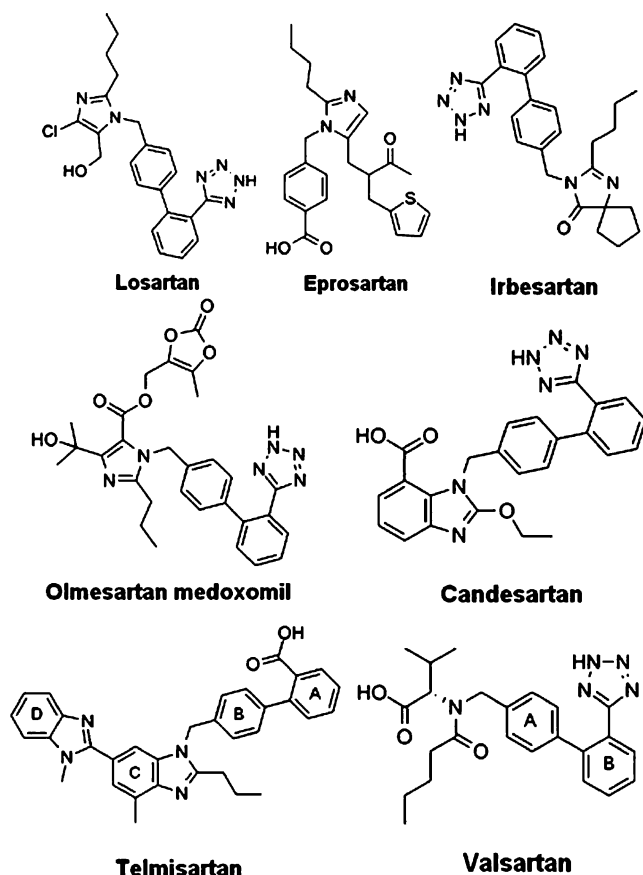

Fig. 2 Chemical structures of angiotensin II (Ang II) receptor blockers (ARBs)

therapeutic action and retard the time of onset [17–19]. Moreover, previous studies revealed that HSA is the main protein bound to ARBs by comparing with α1-acid glycoprotein and gamma globulins both in vitro and in vivo [20, 21]. Due to their high albumin binding properties, any change in the interaction between ARBs and HSA could lead to significant changes in the pharmacologically active concentration of ARBs. For instance, Maillard et al. [22] evaluated the effect of human plasma on the antagonistic activity of two ARBs, tasosartan and enoltasosartan. The presence of plasma protein increased the IC_{50} of these ARBs, especially that of enoltasosartan, with IC_{50} values increasing by up to 1,000 times. However, a detailed understanding of the interactions between HSA and ARBs at a molecular level has not yet been reported.

Several in silico models for the evaluation of drug-binding affinity to HSA have been established using docking and quantitative structure–activity relationship (QSAR) methods [23-25]. In addition, molecular dynamics (MD) simulations have been used successfully to gain insight into the dynamic behavior of HSA–ligand complexes in solution. For example, Díaz et al. [26] studied the effect of different protonation states of Lys195 and Lys199 on the IIA binding site using MD simulation; Fujiwara et al. [27, 28] performed MD simulations on HSA binding with fatty acids, and their recent work has revealed high and low affinity sites for fatty acids on HSA that are in good agreement with experimental results [28].

In the current work, in order to gain insight into the interactions between HSA and ARBs at a molecular level, molecular docking of ARBs to HSA was first performed to identify the binding site. Then, MD simulations were performed on HSA–ARBs complexes in aqueous solution to explore the stabilities and dynamic properties of the binding sites. Our molecular docking and MD simulations revealed interesting features of HSA–valsartan and HSA–

Table 1 Binding energies (kcal mol^{-1}) obtained from molecular docking of human serum albumin (HSA) with angiotensin II (Ang II) receptor blockers (ARBs)

ARB	Lowest binding energy		Mean binding energy	
	Site I	Site II	Site I	Site II
Telmisartan	−10.97	−13.34	−10.31	−12.88
Candesartan	−8.41	−9.69	−8.51	−9.49
Losartan	−10.25	−11.43	−10.15	−10.96
Olmesartan [a]	−10.31	−12.63	−9.43	−12.13
Irbesartan	−9.60	−10.89	−9.41	−10.07
Eprosartan	−10.27	−10.69	−10.11	−9.58
Valsartan	−8.19	−9.66	−7.65	−8.76

[a] Olmesartan represents olmesartan medoxomil

Fig. 3 a,b Most favorable docking structures of ARBs in site II. Based on differences in the positions of biphenyl-acidic groups (tetrazole ring or carboxyl), the binding modes of HSA-ARBs can be divided into two classes: (a) mode I and (b) mode II. Carbon atoms of ARBs: *blue* telmisartan, *orange* eprosartan, *magenta* olmesartan medoxomil, *yellow* valsartan, *white* candesartan, *hotpink* irbesartan, *purple* losartan
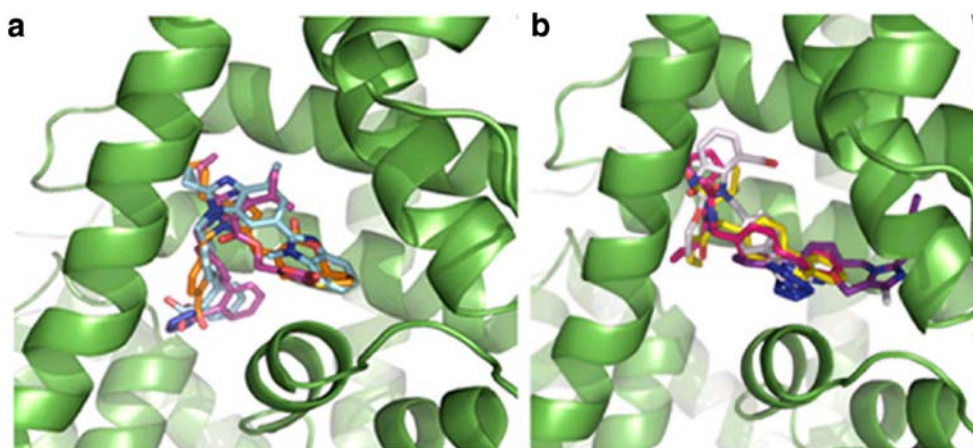
telmisartan binding sites, which will be helpful in designing drugs with appropriate HSA binding affinity.

Computational methods

ARB docking to HSA was performed with the AutoDock 4.0 program using the Lamarckian genetic algorithm [29]. The initial structures of ARBs were obtained from the DrugBank database [30] and were optimized at the HF/6-31G* level. Three-dimensional (3D) crystal structures of HSA complexed with warfarin [31] (PDB code 1H9Z) and with propofol [32] (PDB code 1E7A) were used as starting models. Two grid maps for site I and site II of HSA, centered at the middle of subdomains IIA and IIIA, respectively, were calculated using an $80 \times 80 \times 80$ points rid size with 0.375 Å grid spacing. HSA is held rigid and all the torsional bonds of ARBs are taken as being free during docking calculations. Polar hydrogens for HSA were then added using AutoDock Tools, and Kollman united atom partial charges [33] were assigned. In docking calculations, the preferred conformation obtained from docking depends on selection of the appropriate algorithm and scoring function (based on their energies). Moreover, the protein is usually set to be rigid, and there is no consideration of the effect of solvent molecules on docking. In our docking calculations, 150 docking runs were carried out, and 150 structures of complexes were obtained. Based on the root mean squares (RMS) cluster tolerance (1.5 Å used in this work) between structures, these complexes were sorted into clusters, i.e., different clusters with different HSA binding modes. For example, in the HSA–valsartan docking calculation of site II, we finally obtained 28 clusters. Judging from the values of mean binding energy and number of structures in the cluster, cluster 2 was found to be the preferred binding site as it had the lowest mean binding energy (-8.76 kcal mol^{-1}) and the largest number
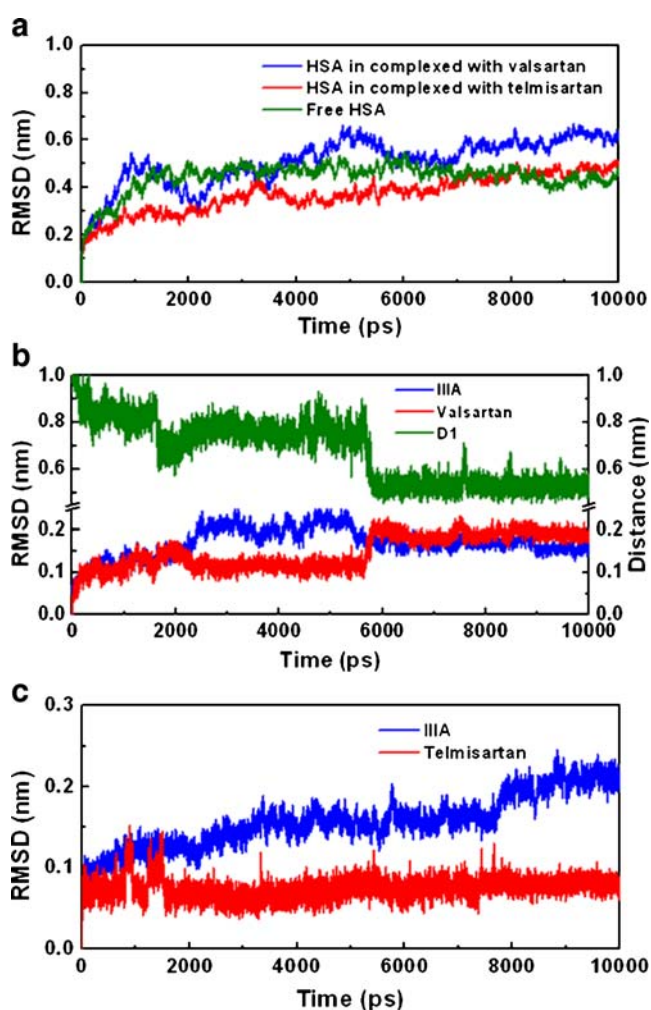

Fig. 4 Time dependence of root-mean square deviations (RMSDs). **a** C_α RMSD for free HSA and bound HSA. **b** RMSD values of HSA subdomain IIIA and valsartan in the HSA–valsartan complex. The center of mass (CM) distance between carboxyl and tetrazole groups of valsartan (trace D1) is also shown for comparison. **c** RMSD values of HSA subdomain IIIA and telmisartan in the HSA–telmisartan complex

of structures (23). Accordingly, the structure with the lowest binding energy in cluster 2 was chosen as the preferred binding mode.

MD simulations were performed on HSA–valsartan and HSA–telmisartan complexes obtained from docking using the Gromacs 3.3.3 package [34, 35] with GROMOS96 force field [36]. The coordinates of ARBs were transferred into Gromacs topologies using the PRODRG [37] algorithm.

Bound and unbound HSA were solvated with water in a cubic periodic box. The SPC/E water model [38] was used and sodium ions were added to neutralize the system. The closest distance from any protein atom to the walls of the box was not less than 10 Å. The LINCS algorithm [39] was used to constrain the bond lengths. Short-range electrostatic and van der Waals forces, with a cutoff radius of 1.0 nm and 1.4 nm, respectively, were calculated for all pairs of a neighbor list, updated every ten steps. Electrostatic interactions were calculated by the Particle Mesh Ewald (pmE) method [40, 41]. To release conflicting contacts, energy minimization was performed using the steepest descent method for 2,000 steps, followed by the conjugated gradient method for 2,000 steps. The position-restrained dynamics simulation of the system, in which the positions of heavy atoms of HSA were restrained by 1,000 kJ mol^{-1} Å^{-2}, was then performed at 300 K for 400 ps. Finally, we performed a 10-ns MD simulation for the system with the NPT ensemble. The periodic boundary condition was used and the motion equations were integrated by applying the leap-frog algorithm with a time step of 2 fs. The pressure was coupled to 1 bar with an anisotropic coupling time of 1.0 ps, and the temperature was kept at 300 K during the simulations with a coupling time of 0.1 ps. Both pressure and temperature were controlled using a Berendsen barostat and thermostat [42].

LIGPLOT [43], a program for automatically plotting protein–ligand interactions, was used to analyze the hydrogen bonds and hydrophobic interactions between HSA and ARBs. Molecular graphics were prepared using PyMOL (Delano Scientific, Palo Alto, CA).

Results and discussion

The docking energies obtained are listed in Table 1. It is clear that site II is more favorable in energy than site I for HSA-ARBs, and that telmisartan has a higher affinity for HSA than valsartan, in agreement with experimental results
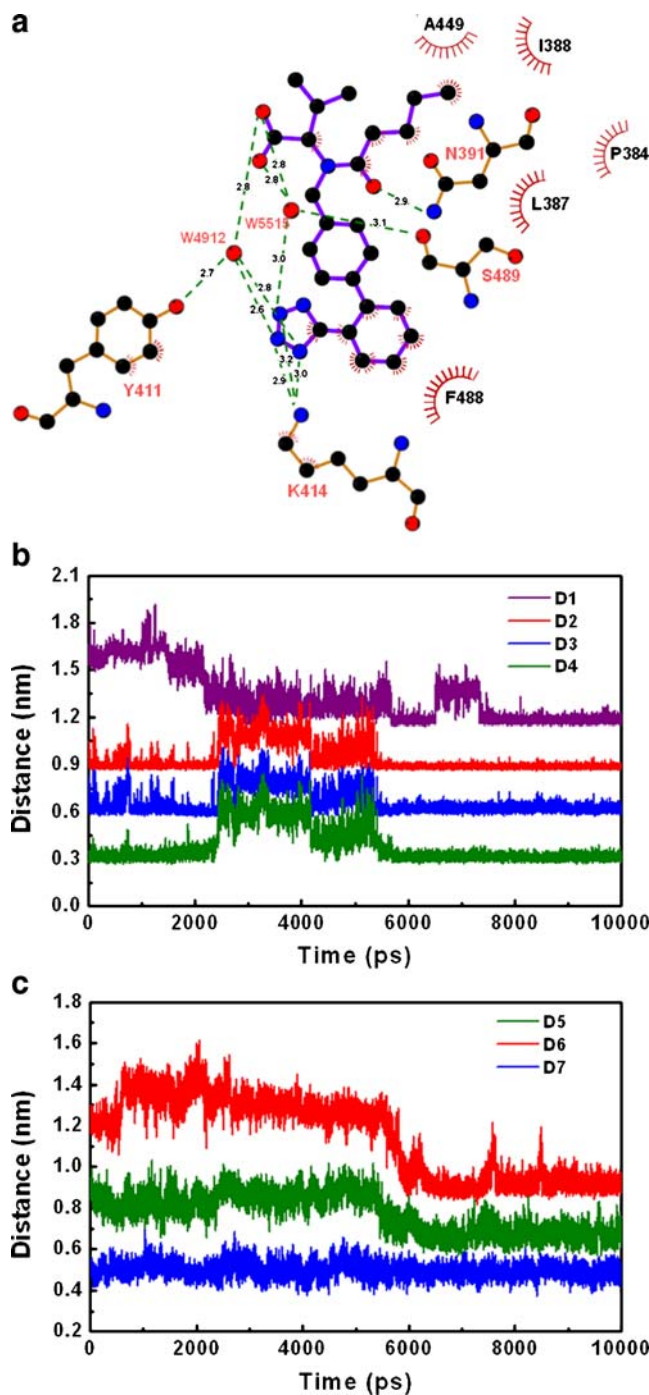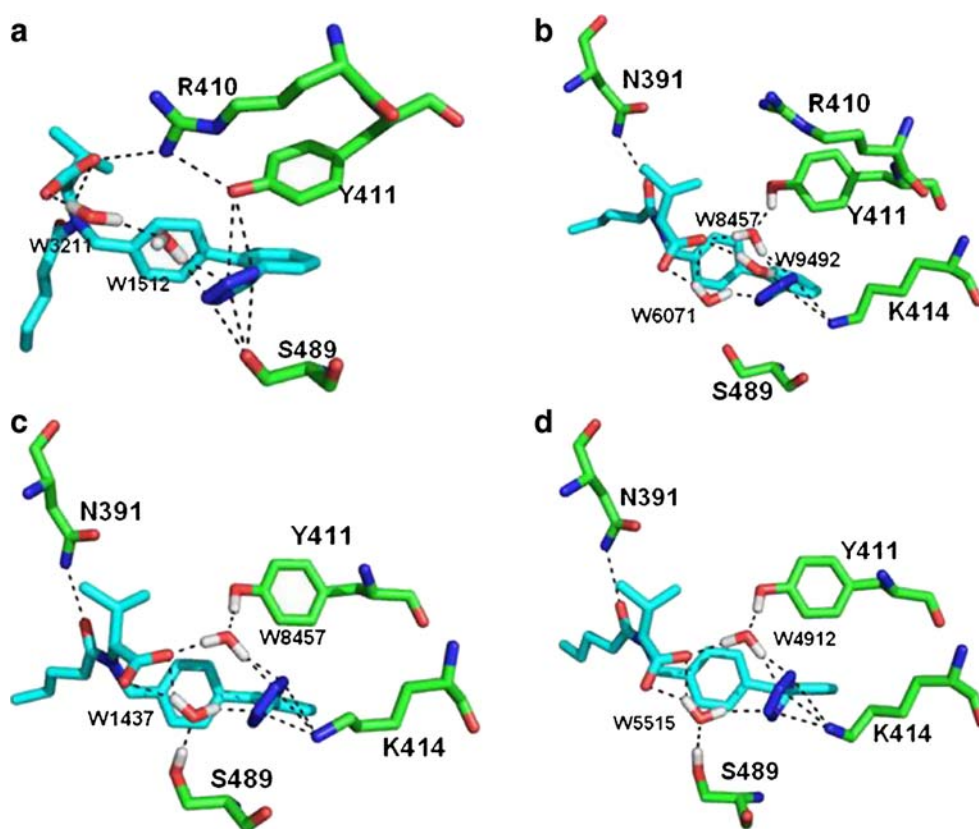

Fig. 5 **a** Two-dimensional schematic representation of hydrogen bond and hydrophobic interactions. *W4912*, *W5515* Water molecules, *dashed lines* hydrogen bonds, *spiked residues* form hydrophobic interactions with valsartan. The figure was plotted using the program LIGPLOT. **b** Time dependence of interatomic distances associated with hydrogen bond interaction of valsartan with HSA in the binding site. Trace *D1* represents the distance between the side chain amidic nitrogen of Asn391 and the ketone oxygen of valsartan; traces *D2*, *D3* and *D4* account for distances between the side chain amidic nitrogen of Lys414 and the tetrazole group of valsartan. To enhance visual clarity, the curves of D1, D2, and D3 are shifted upward by 0.9, 0.6, and 0.3 nm, respectively. **c** CM distances associated with hydrophobic interactions of valsartan with HSA in the binding site with time evolution. Trace *D5* represents the distance between the B-phenyl ring of valsartan and the phenyl ring of Phe488; trace *D6* displays the distance between the butyl group of valsartan and the side chains of Leu387; trace *D7* accounts for the distance between the B-phenyl ring of valsartan and the phenyl ring of Tyr411. The curves of D5 and D6 are shifted upward by 0.2 and 0.4 nm, respectively

[14–16]. The detail binding modes of HSA-ARBs are shown in Fig. S1. Based on differences in the positions of biphenyl-acidic groups (tetrazole ring or carboxyl), the binding modes of HSA-ARBs can be divided into two classes as shown in Fig. 3: (1) the biphenyl-tetrazole (carboxyl) groups locate at the bottom of IIIA and form hydrogen bonds with amino acids of IIB, e.g., HSA–telmisartan, HSA–olmesartan, and HSA–eprosartan; (2) the groups locate between the phenyl groups of Tyr411 and Phe488, e.g., valsartan–HSA, irbesartan–HSA, candesartan–HSA, and losartan–HSA. Compared with mode II, ARBs in mode I more easily form hydrogen bonds with HSA, and the non-biphenyl parts are of the appropriate size to occupy the binding site. The similar U-bend configuration has also been observed in HSA–fatty acid complexes [44]. Analysis of mode II binding sites suggests that the biphenyl groups are located inside the hydrophobic pocket formed by Leu453, Leu457, Leu387, Phe488, Tyr411, and Leu430. In addition, the hydroxyl groups of Tyr411 and Ser489 form electrostatic interactions with the tetrazole rings. Previous reports revealed that Tyr411 could play a key roles in esterase reactions, and covalent and non-covalent drug binding in HSA [45–48]. Compared with other ARBs with mode II binding sites, the non-biphenyl-tetrazole part of losartan has an inverse orientation since its methylene tail occupies a hydrophobic tunnel formed by Leu414, Val426 and Leu460. Moreover, an intramolecular hydrogen bond forms between the hydroxyl and tetrazole groups of losartan.

We took two complexes—HSA–valsartan and HSA–telmisartan, which are representative of complexes with binding sites of mode I and II, respectively—as the initial conformations for MD simulation. MD simulations were performed on these two complexes to investigate the dynamics properties of HSA–ARBs complexes in water.

Initially, the root-mean square deviations (RMSDs) with respect to the starting backbone C_α atom structure for unliganded and liganded HSA were calculated to examine whether each system reaches equilibrium. As shown in Fig. 4a, in each system, RMSD values reach stable values after 2, 6, and 3 ns for free HSA, HSA–valsartan, and HSA–telmisartan, respectively. Figure 4b,c displays the RMSD values of the IIIA subdomain, valsartan, and telmisartan in complexes, respectively. The RMSD values of valsartan increase significantly within 5.5–6 ns, thereafter remaining constant. The RMSD values of subdomain IIIA in the HSA–valsartan complex decrease significantly within 5.5–6 ns, reaching a stable value after 6 ns. A rapid change in RMSD value is always associated with a significant conformational change [49]. It was found that the distance between the center of mass (CM) of the carboxyl and tetrazole groups of valsartan also exhibits a large fluctuation in the same time period (5.5–6 ns) and then stayed constant after 6 ns (Fig. 4b). Therefore, the rapid change in RMSDs of valsartan is related to conformational changes in the carboxyl and tetrazole groups of valsartan. These RMSD results demon-

Fig. 6 Snapshots of the hydrogen bond network in the binding site of HSA-valsartan at 4 ns (a), 8 ns (b), and 10 ns (c) of MD simulation. Carbon atoms: *green* HSA, *cyan* valsartan. *Black dotted lines* hydrogen bonds
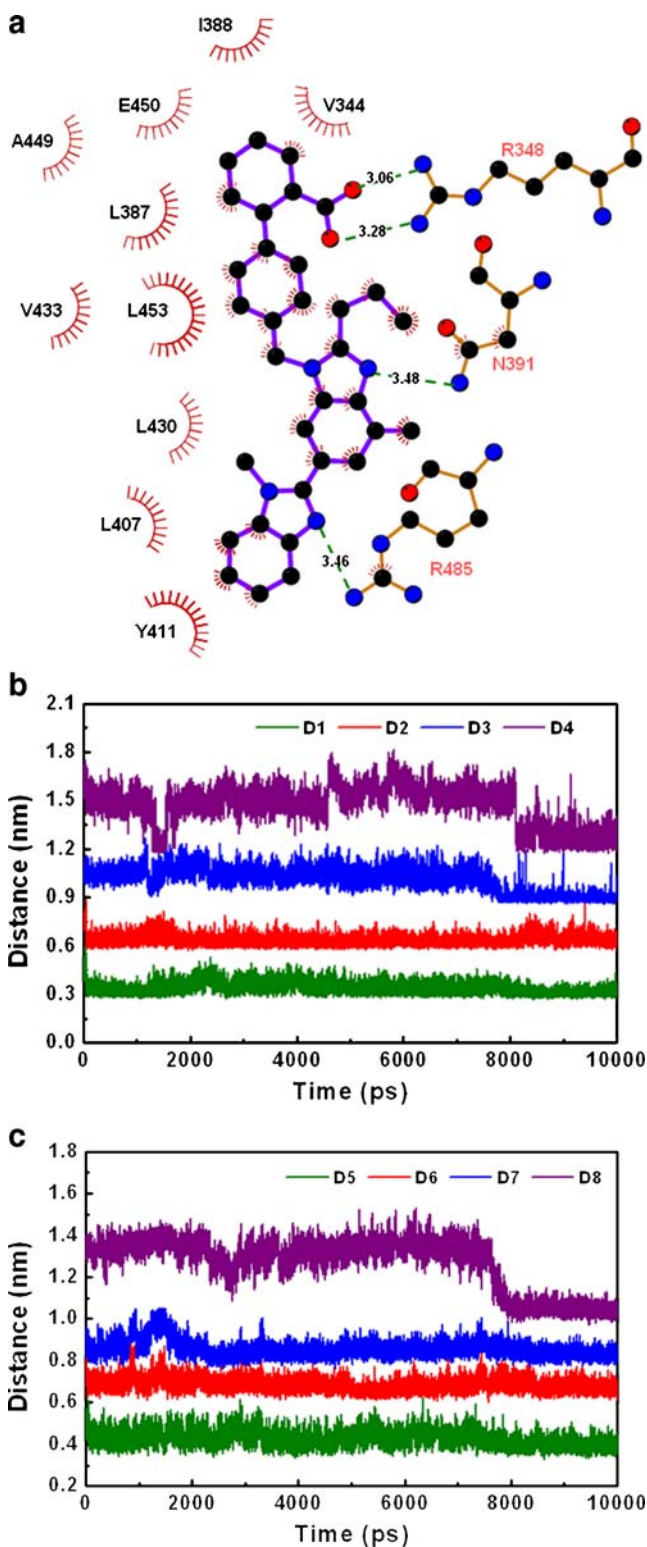
Fig. 7 **a** Two-dimensional schematic representation of hydrogen bond and hydrophobic interactions. *Dashed lines* Hydrogen bonds, *spiked residues/carbon atoms* hydrophobic interactions of HSA–telmisartan. This figure was plotted using the program LIGPLOT. **b** Time dependence of interatomic distances associated with hydrogen bond interactions for the binding site of HSA–telmisartan. Traces *D1* and *D2* represent the distances between the carboxyl oxygen atoms of telmisartan and the side chain amidic nitrogen of Arg348; traces *D3* and *D4* account for the distances from benzimidazole nitrogen atoms of telmisartan to the nitrogen atoms of Asn391 and Arg485, respectively. To enhance visual clarity, the curves of D2, D3, and D4 are shifted upward by 0.3, 0.6, and 0.9 nm, respectively. **c** Time dependence of CM distances associated with hydrophobic interactions in the binding site of HSA–telmisartan. Trace *D5* represents the distance between the phenyl ring of Tyr411 and the D-phenyl ring of telmisartan; trace *D6* displays the distance from the side chain of Leu453 to the C-phenyl ring; trace *D7* represents the distance between the side chain of Val344 and the A-phenyl ring; trace *D8* accounts for the distance between Leu387 and the propyl group of telmisartan. The curves of D6, D7, and D8 are shifted upward by 0.2, 0.4, and 0.6 nm, respectively

values of subdomain IIIA increase significantly within 7.5–8 ns, remaining constant thereafter. The RMSD values reveal that telmisartan does not exhibit a large conformational change when it combines with HSA. Therefore, the U-bend configuration of telmisartan is already quite well suited to the IIIA subdomain pocket.
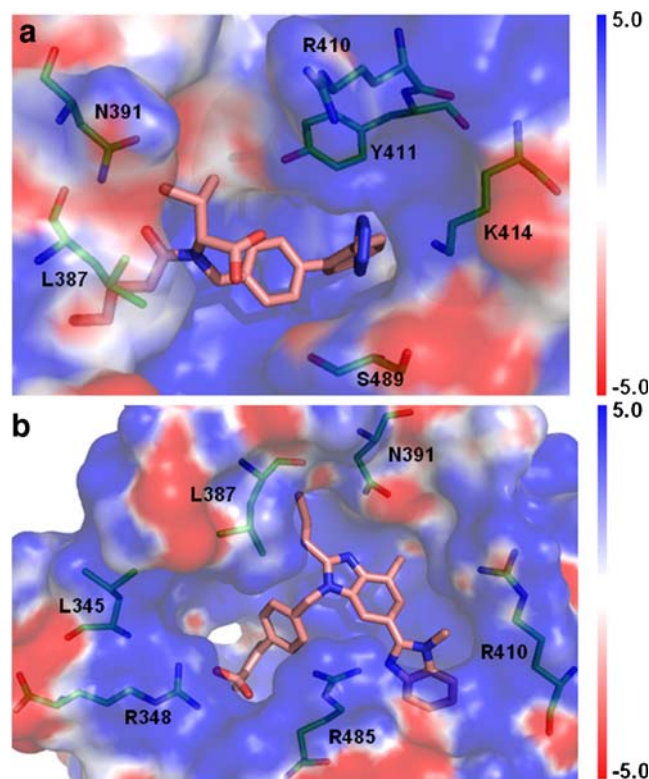
strate that, for the HSA–valsartan complex, both subdomain IIIA and valsartan exhibit conformational changes within 5.5–6 ns, and the HSA–valsartan complex reaches a stable conformation after 6 ns. For HSA–telmisartan, RMSD

Fig. 8 Electrostatic potentials (−5 to +5 kT/e) for binding sites of HSA–valsartan (**a**) and HSA–telmisartan (**b**). *Red* Negative regions, *blue* positive regions, *white* neutral regions

Fig. 9 Final conformations of
the binding sites of HSA–
valsartan (**a**) and HSA–
telmisartan (**b**) after 10 ns
molecular dynamics (MD)
simulation. Carbon atoms:
green HSA, *pink* ARBs. *Black
dotted lines* Hydrogen bonds
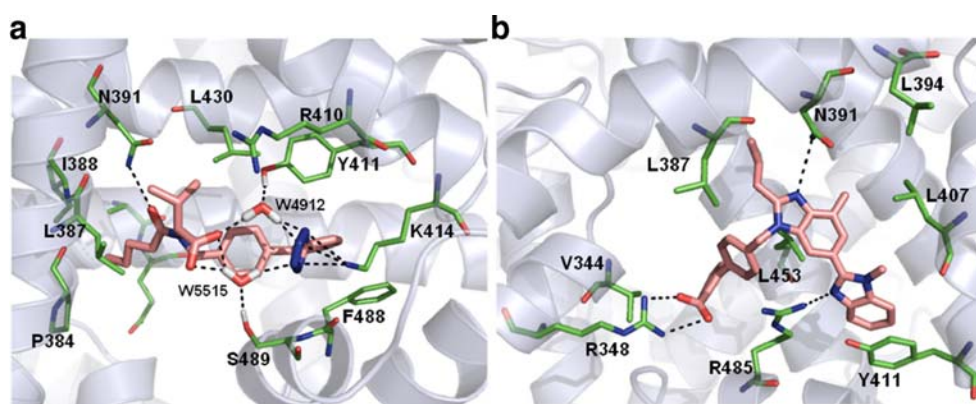
LIGPLOT was used to explore the hydrogen bonds and
hydrophobic contacts between valsartan and HSA as shown
in Fig. 5a; four hydrogen bonds exist between valsartan and
HSA. As shown in Fig. 5, one hydrogen bond forms
between the side chain amide nitrogen of Asn391 and the
ketone oxygen of valsartan (distance D1); the other three
hydrogen bonds are established between the side chain
amine group of Lys414 and the tetrazole group of valsartan
(distance D2–D4). The right side of Fig. 5a shows the
hydrophobic contacts between the benzene ring/side chain
carbon of valsartan and resides (Ala449, Ile388, and
Phe488) of HSA. Figure 5b represents the interatomic
distances between "heavy" atoms associated with H-bonds
with time evolution. The hydrogen-bond distances (D1–D4)
are maintained at around 0.35 nm after 6 ns, which suggests
that hydrogen bond interactions contribute to the stability of
the HSA–valsartan complex. The stabilities of the hydro-
phobic interactions between HSA and valsartan may be
estimated by examining the time dependencies of the
associated CM distances. As shown in Fig. 5c, D5, D6,
and D7 remained constant after 6 ns. This dynamic stability
in the interatomic distances reveals that these hydrophobic
interactions stabilize valsartan in the binding site of HSA.
Moreover, most interatomic distances shown in Fig. 5b,c
fluctuate significantly within 5.5–6 ns, remaining constant
thereafter, which correlates with the RMSDs shown in
Fig. 4b.

Figure 6 represents snapshots of the evolution of the
hydrogen bond network in the binding site of HSA–
valsartan with time. It can be seen that there are hydrogen
bonds between valsartan and the Asn391 and Lys414
residues of HSA. Interestingly, several water molecules
locate around the HSA–valsartan binding site as shown in
Fig. 6. Interestingly, these water molecules join carboxyl/
tetrazole groups of valsartan and two residues (Tyr411 and
Ser489) of HSA together through hydrogen bonds as shown
in Fig. 6b,c. Furthermore, several water molecules in the
hydrogen bond network always exchange with other water
molecules with the time evolution shown in Fig. 6. Clearly,

the presence of these water bridges is important for
stabilizing the configuration of the HSA–valsartan binding
site. However, the binding mode of telmisartan with HSA
(Fig. 7) obtained from MD simulations is different from
that of HSA–valsartan. As shown in Fig. 7a, there are two
hydrogen bonds between the carboxyl moiety of telmisartan
and the side chain of Arg348, which correspond to the
distances D1 and D2 in Fig. 7b. These two hydrogen bonds,
with average lengths of 0.32 and 0.33 nm, respectively,
are stable during the MD simulation. Another two weak
hydrogen bonds form between the benzimidazole groups
of telmisartan and Asn391 (distance D3) and Arg485
(distance D4), respectively. These hydrogen bond distances
remain stable after ~8 ns, and are consistent with the
RMSD changes of HSA subdomain IIIA and telmisartan.
The left side of Fig. 7a notes the hydrophobic contacts
between the benzene rings of telmisartan and the Tyr411,
Leu453, Val344, and Leu387 resides of HSA. Figure 7c
shows the time evolution of the CM distances associated
with hydrophobic interactions of telmisartan in the binding
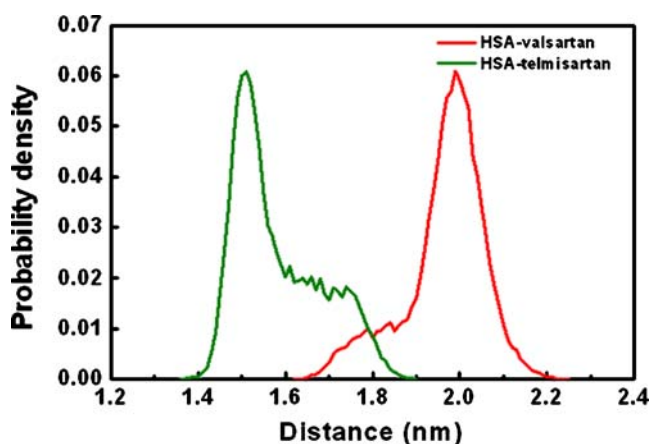site of HSA. Based on the bound structures, hydrophobic

Fig. 10 The distance distribution between Trp214 and ARBs in MD
simulation

interactions appear to play a larger role in HSA–telmisartan binding than in HSA–valsartan binding.

In order to examine the effect of electrostatic interactions on ARB-HSA binding sites, the electrostatic potential of the binding sites were calculated as shown in Fig. 8. It can be seen that the electronegative tetrazole group of valsartan lies in a strongly positive pocket formed mainly by Arg410, Tyr411, Lys414, and Ser489. Similarly, telmisartan, which has a negative charge, locates in a positive pocket consisting mainly of Leu345, Arg348, Arg485, Arg410, Asn391, and Leu387 residues. This demonstrates that electrostatic interactions contribute to binding side formation in ARBs–HSA. The final structures of the HSA–valsartan and HSA-telmisartan binding sites after 10 ns MD simulation are shown in Fig. 9. The conformation of valsartan in HSA–valsartan is similar to that in other protein–valsartan complexes [50, 51].

The molecular distance between Trp214 (donor) and drug (acceptor) is an important binding parameter of HSA–drug complexes, which can be measured by FRET in experimental studies [52–54]. The fluorescence of protein from tryptophan can be quenched by some substrates, and Trp214 located in subdomain IIA is the sole tryptophan residue in HSA. Therefore, the distance distribution between Trp214 and ARBs from the current MD simulations were measured and are shown in Fig. 10. The average distances between Trp-214 and ARBs are 1.96 ± 0.09 nm (for HSA–valsartan) and 1.58 ± 0.10 (for HSA–telmisartan), respectively. The shorter average distance in the latter complex demonstrates a potential for greater energy transfer than in the former complex. This information could be very helpful for further FRET analysis of the bound complexes.

Conclusions

In this work, the binding of ARBs to HSA at the molecular level was investigated and explored by docking and MD simulations for the first time. The docking results revealed that site II (subdomain IIIA of HSA) is more favorable in energy than site I for HSA–ARBs. Also, telmisartan has a higher affinity to HSA than does valsartan, which is in agreement with the available experimental results. The conformations of the HSA–valsartan and HSA–telmisartan binding sites remain stable after 6 and 8 ns MD simulations, respectively. MD simulation results demonstrate that electrostatic interactions appear to be more important than hydrophobic interactions in stabilizing the binding site of HSA–valsartan, while the converse is true for HSA–telmisartan. In addition, the average distances between Trp-214 and ARBs were estimated based on MD simulations, which could be very helpful for future FRET analysis.

It is well known that designing drugs with a desired affinity to HSA is a complicated and difficult task, and researchers have to consider whether modification of the drugs reduces the therapeutic effect. The insights into HSA–ARB binding sites obtained from this work should provide valuable information for the rational design of new ARB drugs.

References

1. Means GE, Bender ML (1975) Acetylation of human serum albumin by p-nitrophenyl acetate. Biochemistry 14:4989–4994
2. He XM, Carter DC (1992) Atomic structure and chemistry of human serum albumin. Nature 358:209–216
3. Carter DC, Ho JX (1994) Structure of serum albumin. Adv Protein Chem 45:153–203
4. Reidenberg MM, Erill S (1986) Drug–protein binding. Praeger, New York
5. Sudlow G, Birkett DJ, Wade DN (1975) The characterization of two specific drug binding sites on human serum albumin. Mol Pharmacol 11:824–832
6. Kearney PM, Whelton M, Reynolds K, Muntner P, Whelton PK, He J (2005) Global burden of hypertension: analysis of worldwide data. Lancet 365:217–223
7. Mancia G, Rosei EA, Cifkova R, DeBacker G, Erdine S, Fagard R, Farsang C, Heagerty AM, Kawecka-Jaszcs K, Kiowski W, Kjeldsen S, Luscher T, McInnes G, Mallion JM, Brien EO, Poulter NR, Priori SG, Rahn KH, Rodicio JL, Ruilope LM, Safar M, Staessen JA, van Zwieten P, Waeber B, Williams B, Zanchetti A, Zannad F (2003) 2003 European Society of Hypertension-European Society of Cardiology guidelines for the management of arterial hypertension. J Hypertens 21:1011–1053
8. Mancia G, Seravalle G, Grassi G (2003) Tolerability and treatment compliance with angiotensin II receptor antagonists. Am J Hypertens 16:1066–1073
9. Cheng QN, Law PK, de Gasparo M, Leung PSJ (2008) Combination of the dipeptidyl peptidase IV inhibitor LAF237 [(S)-1-[(3-Hydroxy-1-adamantyl)ammo]acetyl-2-cyano-pyrrolidine] with the angiotensin II type 1 receptor antagonist valsartan [N-(1-Oxopentyl)-N-[[2′-(1H-tetrazol-5-yl)-[1, 1′-biphenyl]-4-yl]meth-yl]-L-valine] enhances pancreatic islet morphology and function in a mouse model of type 2 diabetes. Pharmacol Exp Ther 327:683–691
10. Katayama K, Nomura S, Ishikawa H, Murata T, Koyabu S, Nakano T (2006) Comparison between valsartan and valsartan plus cilnidipine in type II diabetics with normo- and micro-albuminuria. Kidney Int 70:151–156
11. Aslam S, Santha T, Leone A, Wilcox C (2006) Effects of amlodipine and valsartan on oxidative stress and plasma methylarginines in end-stage renal disease patients on hemodialysis. Kidney Int 70:2109–2115
12. Pfeffer MA, McMurray JJV, Velazquez EJ, Rouleau JL, Kober L, Maggioni AP, Solomon SD, Swedberg K, van de Werf F, White H, Leimberger JD, Henis M, Edwards S, Zelenkofske S, Sellers MA, Califf RM, Investigators VTN (2003) Valsartan, captopril, or

both in myocardial infarction complicated by heart failure, left ventricular dysfunction, or both. N Engl J Med 349:1893–1906

13. Latini R, Masson S, Arland I, Judd D, Maggioni AP, Chiang YT, Bevilacqua M, Salio M, Cardano P, Dunselman P, Holwerda NJ, Tognoni G, Cohn JN, Investigators VH (2002) Effects of valsartan on circulating brain natriuretic peptide and norepinephrine in symptomatic chronic heart failure. Circulation 106:2454–2458

14. Israili ZH (2000) Clinical pharmacokinetics of angiotensin II (AT1) receptor blockers in hypertension. J Hum Hypertens 14: S73–S86

15. Ruilope L (1997) Human pharmacokinetic/pharmacodynamic profile of irbesartan: a new potent angiotensin II receptor antagonist. J Hypertens 15:S15–S20

16. Gardner SF, Franks AM (2003) Olmesartan medoxomil: the seventh angiotensin receptor antagonist. Ann Pharmacother 37:99–105

17. Kratochwil NA, Huber W, Muller F, Kansy M, Gerber PR (2002) Predicting plasma protein binding of drugs: a new approach. Biochem Pharmacol 64:1355–1374

18. Mao HY, Hajduk PJ, Craig R, Bell R, Borre T, Fesik SW (2001) Rational design of diflunisal analogues with reduced affinity for human serum albumin. J Am Chem Soc 123:10429–10435

19. Schmidt B, Schieffer B (2003) Angiotensin II AT1 receptor antagonists. Clinical implications of active metabolites. J Med Chem 46:2261–2003

20. Colussi DM, Parisot C, Rossolino ML, Brunner LA, Lefevre GYJ (1997) Protein binding in plasma of valsartan, a new angiotensin II receptor antagonist. J Clin Pharmacol 37:214–221

21. Christ DD (1995) Human plasma protein binding of the angiotensin II receptor antagonist losartan potassium (DuP 753/ MK 954) and its pharmacologically active metabolite EXP3174. J Clin Pharmacol 35:515–520

22. Maillard MP, Rossat J, Brunner HR, Burnier M (2000) Tasosartan, enoltasosartan, and angiotensin II receptor blockade: the confounding role of protein binding. J Pharmacol Exp Ther 295:649–654

23. Votano JR, Parham M, Hall LM, Hall LH, Kier LB, Oloff S, Tropsha A (2006) QSAR modeling of human serum protein binding with several modeling techniques utilizing structure—information representation. J Med Chem 49:7169–7181

24. Ermondi G, Lorenti M, Caron G (2004) Contribution of ionization and lipophilicity to drug binding to albumin: a preliminary step toward biodistribution prediction. J Med Chem 47:3949–3961

25. Aureli L, Cruciani G, Cesta MC, Anacardio R, de Simone L, Moriconi A (2005) Predicting human serum albumin affinity of interleukin-8 (CXCL8) inhibitors by 3D-QSPR approach. J Med Chem 48:2469–2479

26. Diaz N, Suarez D, Sordo TL, Merz KM (2001) Molecular dynamics study of the IIA binding site in human serum albumin: influence of the protonation state of Lys195 and Lys199. J Med Chem 44:250–260

27. Fujiwara SI, Amisaki T (2006) Molecular dynamics study of conformational changes in human serum albumin by binding of fatty acids. Proteins 64:730–739

28. Fujiwara SI, Amisaki T (2008) Identification of high affinity fatty acid binding sites on human serum albumin by MM-PBSA method. Biophys J 94:95–103

29. Morris GM, Goodsell DS, Halliday RS, Huey R, Hart WE, Belew RK, Olson AJJ (1998) Automated docking using a Lamarckian genetic algorithm and an empirical binding free energy function. J Comput Chem 19:1639–1662

30. Wishart DS, Knox C, Guo AC, Shrivastava S, Hassanali M, Stothard P, Chang Z, Woolsey J (2006) DrugBank: a comprehensive resource for in silico drug discovery and exploration. Nucleic Acids Res 34:D668–D672

31. Petitpas I, Bhattacharya AA, Twine S, East M, Curry S (2001) Crystal structure analysis of warfarin binding to human serum albumin. J Biol Chem 276:22804–22809

32. Bhattacharya AA, Curry S, Franks NP (2000) Binding of the general anesthetics propofol and halothane to human serum albumin. J Biol Chem 275:38731–38738

33. Morris GM, Goodsell DS, Huey R, Olson AJ (1996) Distributed automated docking of flexible ligands to proteins parallel applications of AutoDock 2.4. J Comput Aid Mol Des 10:293–304

34. Berendsen HJC, van der Spoel D, van Drunen R (1995) GROMACS: a message-passing parallel molecular dynamics implementation. Comput Phys Commun 91:43–56

35. Lindahl E, Hess B, van der Spoel D (2001) GROMACS 3.0: a package for molecular simulation and trajectory analysis. J Mol Model 7:306–317

36. Ott KH, Meyer B (1996) Parametrization of GROMOS force field for oligosaccharides and assessment of efficiency of molecular dynamics simulations. J Comput Chem 17:1068–1084

37. Schuettelkopf AW, van Aalten DMF (2004) PRODRG: a tool for high-throughput crystallography of protein–ligand complexes. Acta Crystal D60:1355–1363

38. Berendsen HJC, Grigera JR, Straatsma TP (1987) The missing term in effective pair potentials. J Phys Chem 91:6269–6271

39. Hess B, Bekker H, Berendsen HJC, Fraaije JGEM (1997) LINCS: a linear constraint solver for molecular simulations. J Comput Chem 18:1463–1472

40. Essman U, Perela L, Berkowitz ML, Darden HL, Pedersen LG (1995) A smooth particle mesh Ewald method. J Chem Phys 103:8577–8593

41. Kholmurodov K, Smith W, Yasuoka K, Darden T, Ebisuzaki T (2000) A smooth-particle mesh Ewald method for DL_POLY molecular dynamics simulation package on the Fujitsu VPP700. J Comput Chem 21:1187–1191

42. Berendsen HJC, Postma JPM, van Gunsteren WF, DiNola A, Haak JR (1984) Molecular dynamics with coupling to an external bath. J Chem Phys 81:3684–3690

43. Wallace AC, Laskowski RA, Thornton JM (1995) LIGPOLT: a program to generate schematic diagrams of protein-ligand interactions. Protein Eng 8:127–134

44. Bhattacharya AA, Grune T, Curry S (2000) Crystallographic analysis reveals common modes of binding of medium and long-chain fatty acids to human serum albumin. J Mol Biol 303:721–732

45. Watanabe H, Tanase S, Nakajou K, Maruyama T, Kragh-Hansen U, Otagiri M (2000) Role of Arg-410 and Tyr-411 in human serum albumin for ligand binding and esterase-like activity. Biochem J 349:813–819

46. Li B, Schopfer LM, Hinrichs SH, Masson P, Lockridge O (2007) Matrix-assisted laser desorption/ionization time-of-flight mass spectrometry assay for organophosphorus toxicants bound to human albumin at Tyr411. Anal Biochem 361:263–272

47. Monti S, Manet I, Manoli F, Capobianco ML, Marconi G (2008) Gaining an insight into the photoreactivity of a drug in a protein environment: a case study on nalidixic acid and serum albumin. J Phys Chem B 112:5742–5754

48. Ahmed N, Dobler D, Dean M, Thornalley PJ (2005) Peptide mapping identifies hotspot site of modification in human serum albumin by methylglyoxal involved in ligand binding and esterase activity. J Biol Chem 280:5724–5732

49. Ko S, Lee W, Lee S, Park H (2008) Nanosecond molecular dynamics simulations of Cdc25B and its complex with a 1, 4-naphthoquinone inhibitor: implications for rational inhibitor design. J Mol Graph Model 27:13–19

50. Tuccinardi T, Calderone V, Rapposelli S, Martinelli A (2006) Proposal of a new binding orientation for nNon-Peptide AT1

antagonists: homology modeling, docking and three-dimensional quantitative structure-activity relationship analysis. J Med Chem 49:4305–4316

51. Potamitis C, Zervou M, Katsiaras V, Zoumpoulakis P, Durdagi S, Papadopoulos MG, Hayes JM, Grdadolnik SG, Kyrikou I, Argyropoulos D, Vatougia G, Mavromoustakos T (2009) Antihypertensive drug valsartan in solution and at the AT1 receptor: conformational analysis, dynamic NMR spectroscopy, in Silico docking, and molecular dynamics simulations. J Chem Inf Model 49:726–739

52. Abou-Zied OK, Al-Shihi OIK (2008) Characterization of subdomain IIA binding site of human serum albumin in its native, unfolded, and refolded states. J Am Chem Soc 130:10793–10801

53. Patel S, Datta A (2007) Steady state and time-resolved fluorescence investigation of the specific binding of two chlorin derivatives with human serum albumin. J Phys Chem B 111:10557–10562

54. Zhang G, Keita B, Brochon JC, Oliveira P, Nadjo L, Craescu CT, Miron S (2007) Molecular interaction and energy transfer between human serum albumin and polyoxometalates. J Phys Chem B 111:1809–1814